



# RPPR Final Report

## as of 03-Jan-2023

Agency Code: 21XD

Proposal Number: 80370SMST1  
**INVESTIGATOR(S):**

**Agreement Number: W911NF-22-P-0039**

**Name:** Charles Oden  
**Email:** coden@earthsciencesystems.com  
**Phone Number:** 3038002000  
**Principal:** Y

Organization: **Earth Science Systems, LLC**

Address: 11485 W. I-70 Frontage Rd. Unit B, Wheat Ridge, CO 800331111

Country: USA

DUNS Number: 961439739

EIN:

**Report Date:** 01-Jan-2023

Date Received: 28-Dec-2022

**Final Report** for Period Beginning 02-Jun-2022 and Ending 01-Dec-2022

**Title:** Multi-Mode Concrete Scanner

**Begin Performance Period:** 02-Jun-2022

**End Performance Period:** 01-Jan-2023

**Report Term:** 0-Other

Submitted By: Charles Oden

Email: coden@earthsciencesystems.com

Phone: (303) 800-2000

**Distribution Statement:** 1-Approved for public release; distribution is unlimited.

**STEM Degrees:** 0

**STEM Participants:**

**Major Goals:** A light-weight hand-held scanner is needed that can rapidly make a non-destructive assessment of concrete slabs that are up to six feet thick. The Army's stated goals are to measure material strength over the range 3 to 30 +/-3 ksi, estimate thickness to +/- one foot, and locate metal objects inside the structure. The device should also estimate the density of steel reinforcement (rebar) as well as fiber reinforcement. The time required to make the scan should be less than 10 minutes, and results should be obtained while in the field within a few minutes of the scan.

To address the Army's goals, the research group proposed the following development tasks and tests.

1. Develop a prototype Multi-Mode Scanner that incorporates ground penetrating radar (GPR) and stress wave measurements. Base the scanner on an existing hand-held GPR scanner designed for concrete investigations.
2. Increase the radar power output so that it can investigate concrete structures up to six feet thick.
3. Add a microphone array to the scanner so that it can detect stress waves that propagate through the concrete structure.
4. Build and test different methods for exciting stress waves in concrete slabs.
5. Construct large concrete structures suitable for testing and verifying that the system can achieve the Army's goals.
6. Demonstrate that the scanner can detect the back side of a six foot thick concrete slab.
7. Demonstrate that the scanner can detect metallic objects such as rebar to depths of three feet or greater.
8. Demonstrate that the scanner can measure the velocity of Rayleigh waves traveling along the surface.
9. Demonstrate that compressional wave velocity, modulus of elasticity, and concrete strength can be estimated with sufficient from Rayleigh wave velocity
10. Demonstrate that the scanner can measure the slab thickness using both the impact-echo and GPR methods.
11. Demonstrate that the scanner can detect the presence of metal fibers using GPR.
12. Demonstrate that a survey can be made expediently.

**Accomplishments:** The research team designed a new Multi-Mode Scanner and they built a prototype that incorporates both radar and stress wave sensors. An existing hand-held ground penetrating radar (GPR) scanner that is currently sold for concrete inspections was used as a basis for the new scanner.

The power emitted by the commercial GPR system was increased by nearly 5 times in order to increase the penetration depth. Experiments show that the back side of a 6.5 foot thick concrete structure can be readily detected with GPR. Additionally, it was demonstrated that thin metallic objects like rebar can be detected at depths

# RPPR Final Report

## as of 03-Jan-2023

of four feet, and it is likely that deeper objects can be detected.

To add support for stress wave measurements, an inline array of eight miniature microphones was added to the bottom of the scanner. This gives the scanner the ability to measure the stress wave velocity using surface waves, as well as measure the overall slab thickness using the impact-echo method. Assorted stress wave sources were tested including hand-held hammers and a wheel driven mechanical impactor that was added to the back of the scanner. Although several wheel driven impactor designs were built and tested, it was found that a hand-held hammer provided better data quality. Of the sources evaluated, a small 2.5 lb steel hammer provided good overall results. The hand-held hammer also facilitates more types of measurements than an attached impactor, including surface waves, impact-echo, and tomography.

Several concrete structures were fabricated for testing and evaluating the performance of the Multi-Mode Scanner. These include 1) two large five-foot thick blocks that were cast specifically for this project with different concrete strengths, 2) large stacks of high density blocks with embedded metal objects, 3) a reinforced floor of an existing building designed for large loads, and 4) a small block that was cast with metal fibers.

Test results demonstrate the ability to measure stress wave velocities with repeatability better than 3%, which are then used to calculate shear and compressional wave velocities. Estimates of concrete modulus and strength are then determined with empirical relationships with stress wave velocities. Concrete strength estimates from the Multi-Mode Scanner agree to the values obtained from standard crush tests to within approximately 10%. The thickness of the structures estimated from impact-echo measurements and compressional wave velocity estimates agree to better 10% of the actual thickness. The depth of rebar-like objects, their locations, and slab thicknesses were determined using GPR, and were accurate to 7%. Results also indicate that GPR can detect the presence of metal fibers due to their high reflectivity. Non-metallic fibers cannot be directly detected, but their presence can be inferred when strength estimates are larger than 5,000 psi because large strengths cannot be achieved without the use of fibers. The results in this paragraph exceed the requirements stipulated by the Army.

The scanner weighs about five pounds and can operate for six hours on a rechargeable battery. This operating time will be extended to over eight hours in future work. The scanner is operated in conjunction with a tablet computer using a wireless connection, and the tablet computer contains all of the software needed to analyze the data. Planned software updates will provide results to users within a few minutes of completing the scan. Future development will also take scanner from the prototype stage to production ready.

**Training Opportunities:** Nothing to Report

**Results Dissemination:** Nothing to Report

**Honors and Awards:** Nothing to Report

**Protocol Activity Status:**

**Technology Transfer:** Nothing to Report

### **PARTICIPANTS:**

**Participant Type:** PD/PI

**Participant:** Charles P. Oden

**Person Months Worked:** 2.00

Project Contribution:

National Academy Member: N

**Funding Support:**

**Participant Type:** Co PD/PI

**Participant:** Mija H. Hubler

**Person Months Worked:** 1.00

Project Contribution:

National Academy Member: N

**Funding Support:**

**RPPR Final Report**  
as of 03-Jan-2023

**Participant Type:** Other Professional  
**Participant:** Matthew Ragusa  
**Person Months Worked:** 1.00  
Project Contribution:  
National Academy Member: N

**Funding Support:**

**Participant Type:** Other Professional  
**Participant:** Zachary Luzader  
**Person Months Worked:** 1.00  
Project Contribution:  
National Academy Member: N

**Funding Support:**

**Participant Type:** Other Professional  
**Participant:** Richard Johnson  
**Person Months Worked:** 2.00  
Project Contribution:  
National Academy Member: N

**Funding Support:**

**Partners**

,

I certify that the information in the report is complete and accurate:

Signature: Charles P. Oden

Signature Date: 12/28/22 6:48PM



## Final Technical Report

### Multi-Mode Concrete Scanner – Phase I

---

Army Research Office  
Research Triangle Park, NC 27709



---

Contractor: Earth Science Systems, LLC

Contract: W 911NF22P0039

December 2022

PI: Dr. Charles P. Oden, Earth Science Systems, LLC

Co-PI: Dr. Mija H. Hubler, University of Colorado

NOTICE

This document is disseminated under the sponsorship of the Army Research Office in the interest of information exchange. The United States Government assumes no liability for its contents or use thereof. Any opinions, findings and conclusions, or recommendations expressed in this material do not necessarily reflect the views or policies of the United States Government, nor does mention of trade names, commercial products, or organizations imply endorsement by the United States Government. The United States Government assumes no liability for the content or use of the material contained in this document.

NOTICE

The United States Government does not endorse products or manufacturers. Trade or manufacturers' names appear herein solely because they are considered essential to the objective of this report.

## **Acknowledgments**

The authors would like to acknowledge Dr. Dawanne Poree, Dr. Stephen Lee, Dr. Larry Russell, and Dr. Gregory Spurlock of the U.S. Army's Army Research Office for their support, advice and assistance during this activity. This work was funded by the U.S. Army's STTR program.

# Contents

---

Acknowledgments.....	3
Contents.....	4
Figures.....	5
Tables.....	6
Abstract.....	7
1 Introduction.....	8
1.1 Ground Penetrating Radar.....	8
1.2 Elastic Surface Waves.....	10
1.3 Concrete Material Properties.....	12
1.4 Impact Echo.....	12
2 Objectives and Findings.....	14
2.1 Increased Power GPR.....	14
Findings.....	14
2.2 Microphone Array.....	14
Findings.....	15
2.3 Stress Wave Excitation.....	15
Findings.....	15
2.4 Construct Large Concrete Structures.....	16
Findings.....	16
2.5 Demonstrate GPR Performance.....	19
Findings.....	19
2.6 Surface Wave Performance.....	21
Findings.....	21
2.7 Estimating Elastic Properties.....	21
Findings.....	21
2.8 Impact Echo Performance.....	22
Findings.....	22
2.9 Detecting the Presence of Metal Fibers.....	23
Findings.....	23
2.10 Expediency of Scan.....	23
Findings.....	24
3 Conclusions.....	24
4 References.....	26
5 Abbreviations and Acronyms.....	27

## Figures

---

Figure 1. A cross section resulting from a GPR survey (left) and a 3D view (right).....	9
Figure 2. Schematic showing compressional, shear, and Rayleigh waves generated by a impulsive load on the surface (left). Numerical simulation results showing the leaky Rayleigh wave (right). Adapted from Zhu and Popovics (2008).....	10
Figure 3. White areas on coherence diagram indicate the frequencies and velocities of surface wave energy. The orange line is the Rayleigh wave velocity, and the green and red lines are the shear and compressional velocities calculated from the Rayleigh velocity.....	11
Figure 4. Impact-echo simulations showing waves in space above the concrete (left) and received waveforms from an array of microphones (right). Adapted from Groschup and Grosse (2015)....	13
Figure 5. Impact-echo spectral response, peak frequency, and thickness estimate for a 5 foot (1.52 m) thick poured concrete slab .....	14
Figure 6: The Multi-Mode Scanner is an ESS GPR Concrete Scanner (left) that has been modified to have an impactor mechanism (center) and an array of microphones (right).....	15
Figure 7: Conducting an GPR scan on a poured block (left), MASW scan (center), and a collapsed form showing internal reinforcements (right).....	17
Figure 8: Conducting a GPR scan on the composite block (top left), composite block S2 with vertical copper strip (top right), and composite block S3 with vertical copper strip (bottom).....	18
Figure 9: Form for a small concrete block with a rebar grid (left), and completed block that was cast using a mix containing metallic fibers (right).....	18
Figure 10: GPR cross sections for composite blocks S1 and S2.....	19
Figure 11: GPR cross sections for composite blocks S3 and S4.....	20
Figure 12: GPR cross-sections from 750 MHz antennas for poured block P3, with the depth corrected section on the left, and the same section with background correction on the right.....	21
Figure 13: GPR cross-section from 2 GHz antennas for small block with metal fibers.....	23
Figure 14: GPR scanning with scan grid on printed mat (left) and drawn scan grid (right).....	24

# Tables

---

Table 1. Range of Concrete Properties.....12

Table 2. Response of various hammers.....16

Table 3. Parameters of poured concrete blocks.....17

Table 4. Dimensions of composite block structures used to test GPR penetration depth.....17

Table 5. Measured Rayleigh velocity, calculated concrete strength, and 28 day strength test results.....22

Table 6. Measured slab thickness using the IE method.....22

Table 7. Target performance metrics and actual results.....25

## Abstract

A prototype hand-held concrete scanner that combines both ground penetrating radar and elastic wave measurements (such as impact-echo and surface wave) has been built and tested. Such a scanner is not currently commercially available and is anticipated to be a successful product in both the government and private sector markets. This multi-mode scanner will help managers, inspectors, and investigators assure public safety for the operation of a wide variety of structures such as bunkers, buildings, dams, roads, bridges, embankments, and manufacturing plants. The new scanner has the ability to find the important structural parameters such as rebar location, cover, thickness, and material strength.

The new scanner is called the Multi-Mode Scanner and is based on an existing product marketed as the ESS GPR Concrete Scanner. This device uses two sets of radar antennas at different frequencies, 2 GHz and 750 MHz, to provide high resolution and deep penetration respectively for concrete inspection. The Concrete Scanner is a wireless hand-held scanner that uses a tablet PC for data acquisition, data analysis, and report generation. The system provides advanced, fast, and complete analysis in the field. A microphone array has been added to the bottom of the scanner to detect stress waves propagating in the surface, which enables surveys such as multi-channel analysis of surface waves (MASW) and impact-echo (IE) to determine elastic wave velocity and thickness of the structure. Software has been written to acquire and analyze data for MASW and IE surveys. Combining this new software with existing GPR software, users can map the location and depth of rebar, measure the thickness of the structure, and estimate the strength of the concrete.

Several large concrete structures were built for the purpose of testing the performance of the Multi-Mode Scanner. The GPR sensors were tested on concrete structures with thicknesses ranging from 2 to 6.5 feet thick, and it was determined that the device can determine the concrete thickness in structures 6.5 feet thick or more, and detect and locate rebar at depths of 4 feet or more. The MASW measurements successfully measured stress wave velocities which were then used to estimate the concrete strength using empirical relationships. Lastly, the device measured slab thickness using the IE method. The errors between independent and Multi-Mode Scanner measurements of rebar depth and location, slab thickness, and concrete strength were approximately 10% or less for all measurements, which exceeds the Army's stated requirements.

The hand-held scanner weights five lbs. (2.3 kg) and a survey can be conducted in less than 10 minutes for horizontal surfaces. For vertical surfaces, a better method for marking out or affixing a scan grid is needed because current practices can cause survey times to increase to more than 20 minutes. Easy-to-use solutions to this initial shortcoming are planned in subsequent work.

# 1 Introduction

This final report summarizes the work and results obtained in the Phase I project titled "Nondestructive Concrete Characterization System" by Earth Science Systems, LLC (ESS, contractor) and the University of Colorado (CU, subcontractor). The main objective of this project is to develop a portable and non-destructive inspection system utilizing ground penetrating radar (GPR) to provide quick and non-destructive structural analysis of concrete structures. GPR is used routinely to measure the location of embedded reinforcing bars (i.e., rebar), rebar cover, and thickness of slabs. However many commercially available devices designed for concrete scanning are limited to investigation depths on the order of two feet and cannot reach the target depth of six feet. Furthermore, GPR is not able to measure the strength of concrete or detect thin cracks (delaminations) in the structure. To reliably obtain strength properties with a non-destructive method, a measurement of the elastic properties is needed that enables methods such as impact echo (IE), multi-channel analysis of surface waves (MASW), or elastic wave tomography.

This research is needed because currently there are no commercially available scanners that reliably and quantitatively create images of both concrete strength and rebar location from a single scan pass. Such a scanner would enjoy commercial success because the industry already widely uses both GPR and elastic wave methods for the structural analysis of concrete structures. Applications include conducting structural analysis and assessing the health of bunkers, bridge decks, foundations, piers, buildings, dams, and other concrete structures. On the societal level the proposed research aims to reduce the risk, environmental, and public safety impacts caused by deteriorating, failed, or collapsed structures.

The ability of radar and elastic waves to penetrate concrete structures depends on several factors. Radar wave attenuation is a function of water content, maturity, aggregate size, and the presence of distributed conductive materials such as salt or metallic fibers. For mature structures, large aggregate can cause scattering which can reduce penetration depths, and the presence of metallic fibers can reduce the penetration depth to less than 6 inches (15 cm). Elastic waves do not have these depth limitations, but their propagation can be interrupted by voids, cracks, and delaminations (yet they excel at detecting these objects). The combination of radar and elastic wave surveys provides a resilient combination for investigating thick structures to their full depth while also being able to resolve reinforcing structure. GPR is excellent for detecting steel reinforcements, imaging the location of strength members, and is the only technology available for detecting glass bar reinforcements.

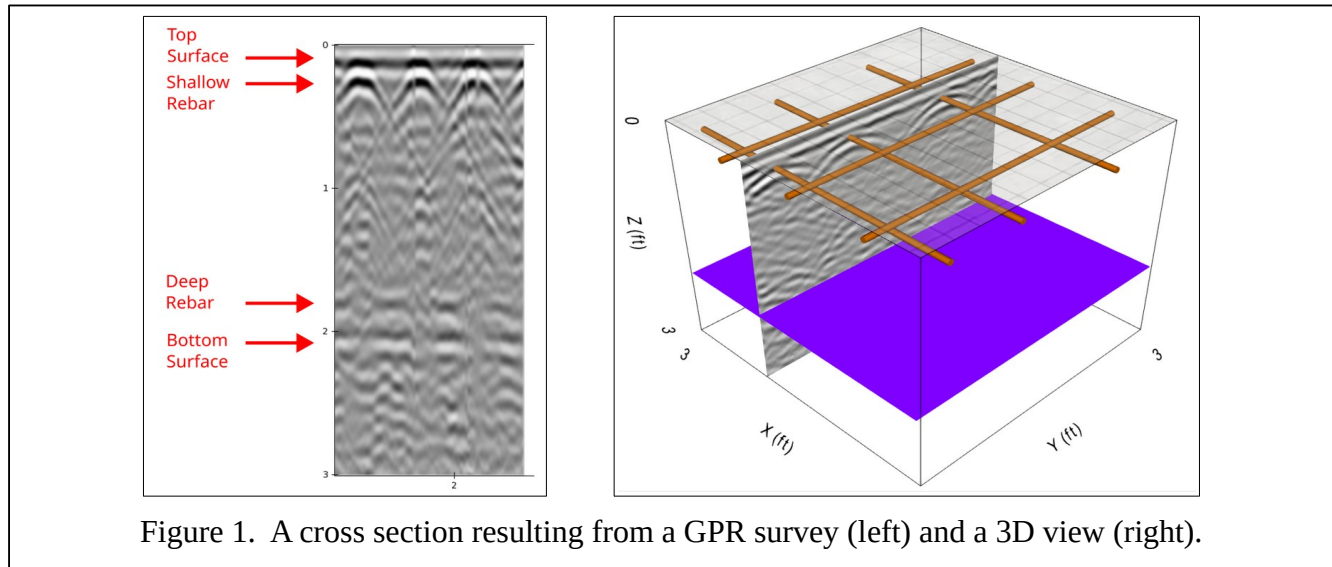
This report starts by providing an overview of the technologies used by the Multi-Mode Scanner in Section 1. Then the objectives and findings are discussed in Section 2. Readers familiar with GPR and stress wave methods may choose to skip the background material in Section 1 and move on to the research results in Section 2. Finally, Section 3 provides conclusions from this research project.

## 1.1 Ground Penetrating Radar

GPR is a non-destructive method that is well-suited for finding reinforcing bars in concrete, voids, and measuring slab thickness. For example Figure 1 shows a cross section obtained from a survey using the ESS GPR Concrete Scanner on a two foot thick concrete floor, as well as a 3D view with the reinforcement bars and bottom of the slab shown as iso-surfaces. Conventional GPR systems designed for concrete inspection are typically able to image to depths of about two feet.

GPR scanners emit impulses of electromagnetic (EM) waves into the medium under test, which are reflected off of material interfaces where the electrical properties of the medium change. Images of

the subsurface are constructed by measuring the travel time of the waves and amplitude of the reflections. For concrete structures, the most common changes occur at boundaries between concrete and steel (rebar), and concrete and air. The change in electrical properties at concrete-steel interfaces is large, which makes the GPR method excellent for detecting and locating rebar. The change in properties at concrete-air interfaces is much weaker and only interfaces with a large surfaces area can be detected such as large voids and edges of the concrete structure. Cracks generally cannot be detected using GPR.



Running GPR along a single scan line produces a cross-section image such as those shown in Figure 1. The horizontal axis on the cross-section images is the scanner location along the scan line, and the vertical axis is depth to the reflector. In the unprocessed GPR data the vertical axis on the cross-section images is wave travel time which was converted to depth after determining the radar wave velocity in the concrete. To measure the velocity, the hyperbolic reflection pattern from a rebar that is oriented perpendicular to the cross-section is examined, whose shape depends on velocity. A hyperbolic shape is calculated using a velocity that makes the shape match the reflection pattern in the image. After the velocity has been determined, the vertical axis can be converted from travel-time to depth, and the depth to rebar and the slab thickness are indicated directly on the cross-section by their reflections. The radar wave velocity,  $v_{em}$ , depends on the dielectric constant,  $\epsilon_r$ , of the concrete according to Equation 1.

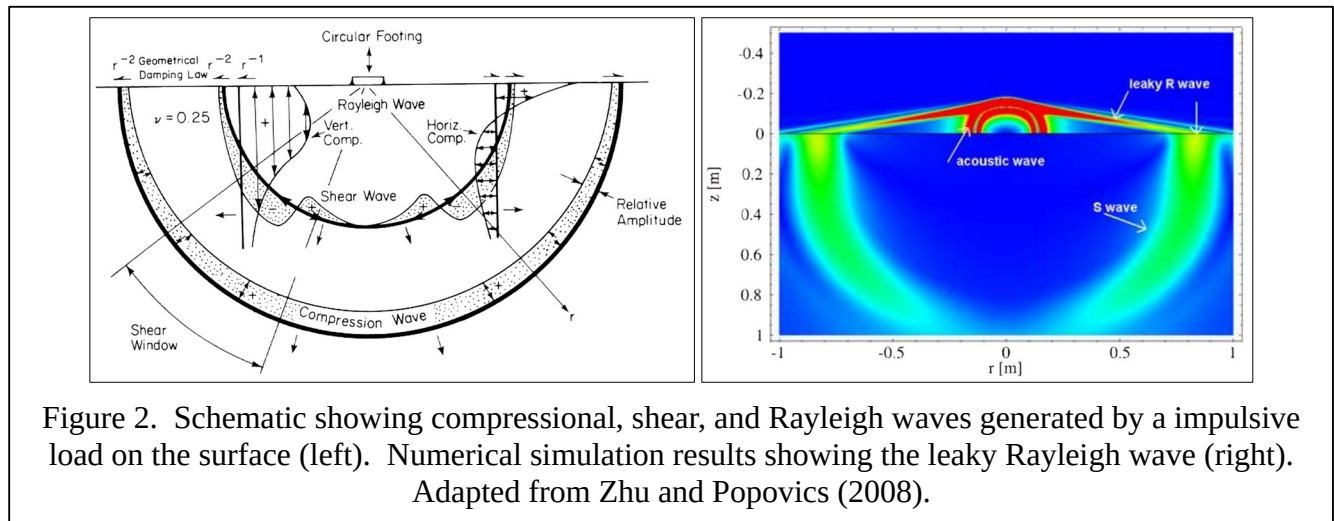
$$v_{em} = \frac{3 \cdot 10^8}{\sqrt{\epsilon_r}} \text{ (m/s)} \quad (1)$$

The dielectric constant of fully cured concrete typically ranges from 4.5 to 7, and for young or water saturated concrete the value is typically lies between 10 and 20. Because young concrete absorbs radar waves, the radar wave penetration depth is often severely limited until the concrete has fully cured.

It is not possible to directly measure the diameter of rebar by examining the reflected radar waves. However, if one rebar is placed directly on top of another, then the rebar diameter can be determined by subtracting their depths.

## 1.2 Elastic Surface Waves

The use of an array of non-contacting microphones to make surface wave measurements of elastic waves was studied by Zhu and Povovics (2008). Elastic waves induced in a thick concrete slab by an impact at the surface generate compressional and shear body waves that travel through the medium, and Rayleigh waves that travel along the surface (see Figure 2). The shear wave velocity is about 10% faster than the Rayleigh wave, and the compressional wave is about 60% faster than the shear wave (assuming a Poisson's ratio of 0.2). The compressional, shear, and Rayleigh waves all produce leaky waves that enter the air above the surface, but the amplitude of laterally propagating leaky compressional and shear waves is negligible. This leaves only the direct acoustic wave and the leaky Rayleigh waves in the air that can be easily detected using microphones. Rayleigh wave amplitude decays exponentially with depth, with higher frequencies sampling the shallow regions and lower frequencies sampling deeper horizons. In heterogeneous media the velocity changes with frequency (or sampling depth), but with largely homogeneous media such as typical concrete structures the velocity remains essentially constant. For thin slabs, plate modes (i.e., Lamb waves) are induced whose velocities change with frequency and approach Rayleigh velocities at high frequencies.



The multi-channel analysis of surface waves (MASW) method employs an array of receivers (microphones) to measure the frequency dependent velocity of waves traveling along a surface. Processing of MASW data starts by filtering the data and then generating a coherence diagram – usually by the phase shift method (Park et al., 1998). The coherence diagram indicates the frequencies and velocities where wave energy occurs (see Figure 3). This is an image with  $n$  discrete frequencies and  $m$  discrete velocities. The coordinate system used for the MASW analysis places the origin at the first receiver location, the  $x$ -axis along the receiver array, the  $z$ -axis positive down, and the  $y$ -axis defined to make a right handed system. The first step is to apply a Fourier transform and series of bandpass filters with center frequencies,  $f_n$ , equally spaced over the frequency range of interest (see Equation 2),

$$R_l^f(f_n, \omega) = F(f_n, \omega) \int R_l(t) e^{-i\omega t} dt . \quad (2)$$

Here,  $\omega$  is radian frequency,  $R_l(t)$  is the time-domain waveform from the  $l$ -th receiver, and  $F(f_n, \omega)$  is a zero-phase Hanning window bandpass filter centered at frequency  $f_n$  with a bandwidth equal to twice

the frequency interval. Next, a coherence image  $C(v_m, f_n)$  is generated from phase shifted receiver pairs using the offset  $x_{jk}$  between them and the test velocity  $v_m$ ,

$$C(v_m, f_n) = \left\| \sum_{j,k} \int R_j^f(f_n, \omega) R_k^f(f_n, \omega) e^{i\omega x_{jk}/v_m} e^{i\omega t} d\omega \right\|. \quad (3)$$

The summation in Equation 3 is over the set of all combinations of receiver pairs. Contributions to the sum in Equation 3 are omitted when spatial aliasing occurs, namely when the distance,  $x_{jk}$ , between receiver pairs is greater than the wavelength,  $v_m/f_n$ , at image location  $m,n$ . Finally, the Rayleigh wave phase velocity,  $v_n$ , at each frequency,  $f_n$ , is selected as the test velocity,  $v_m$ , where  $C(v_m, f_n)$  is maximum. The routine to pick the dispersion curve velocities from the coherence image attempts to extract a continuous curve without sudden offsets to avoid jumping to a different mode. In the coherence diagram shown in Figure 3, the Rayleigh wave dispersion curve is used to calculate the shear and compressional wave velocities using equations presented in the next section.

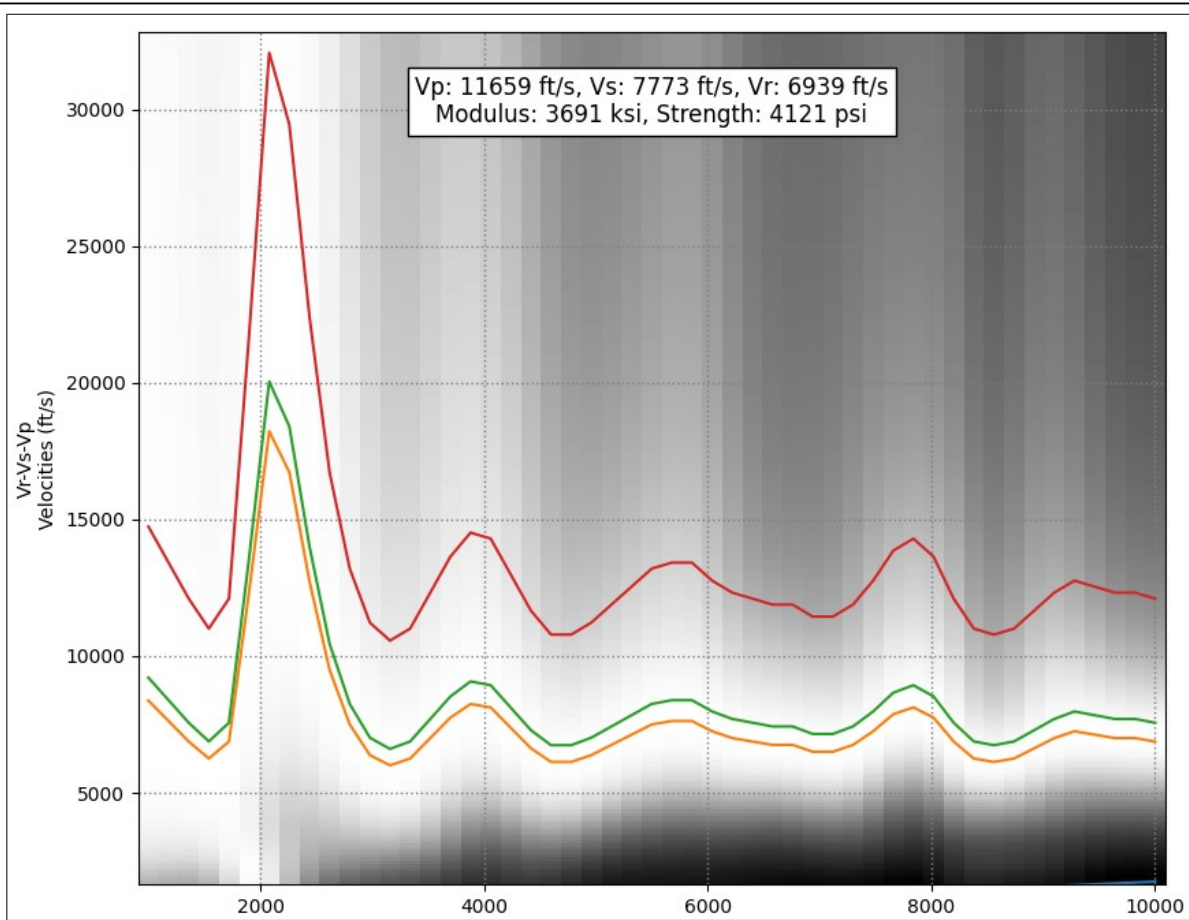


Figure 3. White areas on coherence diagram indicate the frequencies and velocities of surface wave energy. The orange line is the Rayleigh wave velocity, and the green and red lines are the shear and compressional velocities calculated from the Rayleigh velocity.

### 1.3 Concrete Material Properties

The compressive strength of concrete is well correlated with compressional and shear velocities (Lee et al., 2017; Sabbag and Uyanik, 2017; He and Senetakis, 2016; Trtnika et al., 2009). The empirical relationships between elastic moduli and strength in composite materials have been studied for years (Park et al., 2019) and are routinely used to estimate strength from measured elastic properties. The American Concrete Institute (ACI) provides empirically derived relationships between concrete modulus of elasticity, compressive strength, and tensile strength that are routinely used in the design of concrete structures (ACI Code 318-05). Vu et al. (2021) have investigated the relationships between concrete strength and modulus for a wide range of concrete types and sample sizes.

Table 1. Range of Concrete Properties

Property	Weak Concrete Value	Strong Concrete Value
Poisson's Ratio	0.2	0.1
Rayleigh Velocity	3937 ft/s (1200 m/s)	9186 ft/s (2.8 km/s)

The typical ranges of concrete properties are listed in Table 1. After measuring the Rayleigh velocity ( $v_r$ ), the value of Poisson's ratio ( $\nu$ ) is estimated by interpolating between the weak and strong concrete values listed in Table 1. Next, the shear ( $v_s$ ) and compressional ( $v_c$ ) velocities can be calculated using theoretical relationships shown in equations 4 and 5:

$$v_s = v_r \cdot \frac{1 + \nu}{0.87 + 1.12 \nu}, \quad (4)$$

$$v_p = v_s \cdot \sqrt{\frac{1 - \nu}{0.5 - \nu}}. \quad (5)$$

Next, the compressive strength ( $f'_c$  in psi) and Young's modulus ( $E_c$  in psi) are calculated using empirical relationships shown in equations 6 and 7:

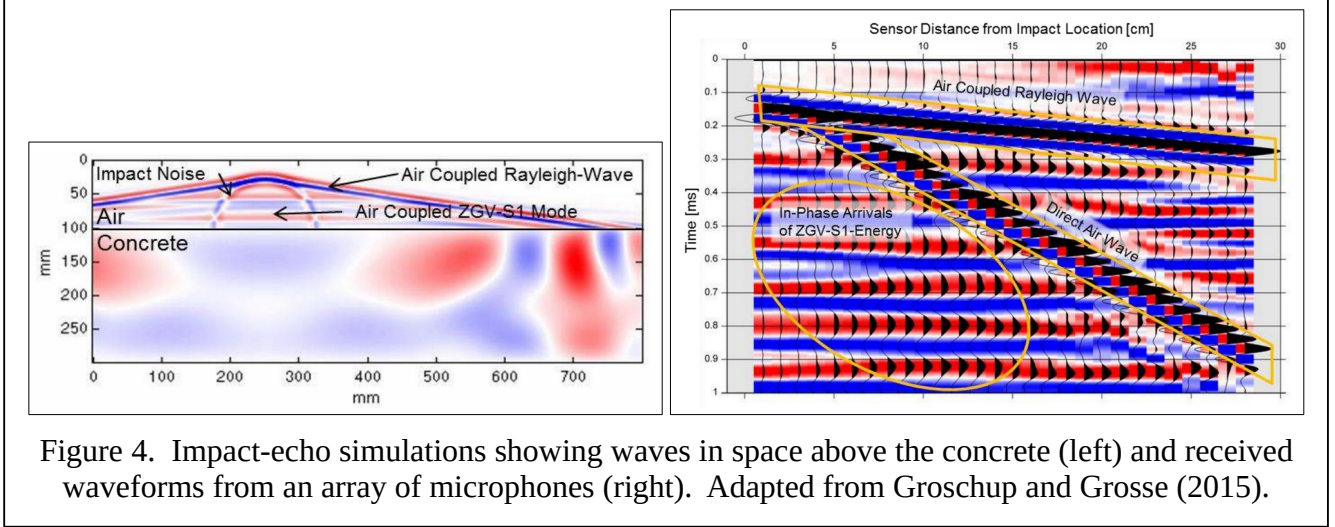
$$f'_c = 145.038 e^{(v_p - 743.88)/839.57}, \quad (6)$$

$$E_c = 57500 \sqrt{f'_c}. \quad (7)$$

### 1.4 Impact Echo

The initial understanding of the impact-echo (IE) method assumed that compressional waves reverberate between the top and bottom of a plate like structure, and a resonant response is observed whose frequency is related to the compressional velocity and thickness (Sansalone and Carino, 1986). More recently, Gibson and Popovics (2005) showed that the impact-echo response is in fact a zero-group-velocity first-symmetrical-mode Lamb wave (ZGV-S1). Although leaky compressional waves in air resulting from waves traveling laterally in concrete are very weak (Sansalone and Carino, 1986), it is possible to make impact-echo measurements using an array of microphones (Groschup and Grosse, 2015) because Lamb waves provide the vertical displacement at the surface that couple to the air. The signals recorded by the microphones include ambient noise, the direct air wave from the hammer

source, leaky Rayleigh waves, and the ZGV-S1 wave (see Figure 4). All of these sound waves travel across the surface at some velocity except the ZGV-S1 wave, and applying a finite velocity filter to the receiver array will attenuate all waves except the ZGV-S1 wave. The hammer used for the impact echo measurement should excite the ZGV-S1 resonant frequency of the slab, with more massive hammers needed for thicker slabs to excite their lower resonant frequencies .



To use microphone recordings for IE measurements, the first step is to apply a filter to remove air waves and surface waves that propagate laterally, which can be accomplished using a 2D Fourier transform filter. Equation 8 calculates the frequency domain response of the filtered wave field using the receiver (microphone) recordings,  $R(x, t)$ , at location,  $x$ , and time  $t$ ,

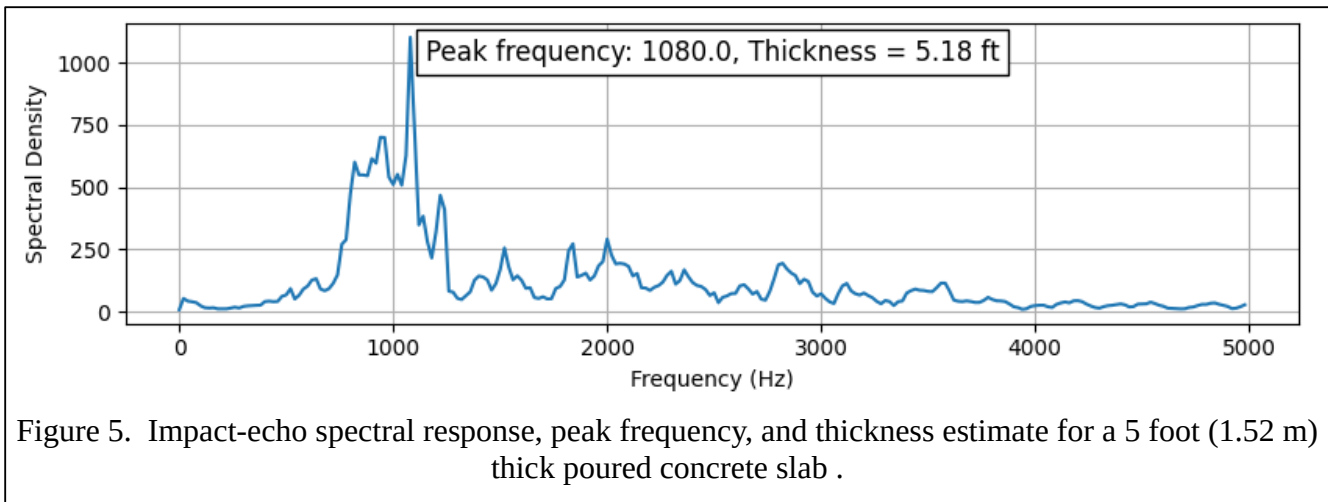
$$R(k_x, \omega) = \left( \int \int R(x, t) e^{ik_x x} e^{-i\omega t} dx dt \right), \text{ if } k_x x > 250, \text{ else } 0, \quad (8)$$

where  $k_x$  is the wave number and  $\omega$  is radian frequency. Equations 9 and 10 are used to calculate the spectral density,  $S$ , where receiver  $j$  is located at  $x_j$ . The peak value of the spectral density occurs at frequency  $f_m$ , which is used to calculate the slab thickness,  $d$ , using the compressional velocity  $v_p$  and Equation 11 (see Figure 5). When using direct contact sensors for IE surveys, the compressional wave velocity is measured directly, but this is not feasible with air coupled microphones and for the later case the velocity is determined using Equation 5.

$$R_j(\omega) = \int R(k_x, \omega) e^{-ik_x x_j} dk_x, \quad (9)$$

$$S(\omega = 2\pi f) = \sum_j \|R_j(\omega)\|. \quad (10)$$

$$d = 0.475 v_p / f_m. \quad (11)$$



## 2 Objectives and Findings

This Section discusses the project's objectives and findings. The project started with an existing ESS product, the GPR Concrete Scanner, which is a wireless hand-held scanner that uses a tablet PC and ESS software for data acquisition and data analysis. The system provides advanced and complete analysis quickly in the field using the GPR method. Stress wave sensors were added to the Concrete Scanner to create the prototype Multi-Mode Scanner, which was subjected to various performance tests as described in the sub-sections below. The sub-section headings correspond to the stated objectives of the project.

### 2.1 Increased Power GPR

The GPR Concrete Scanner enjoys better depth penetration than other GPR products on the market because it contains a 2 GHz antenna pair for high resolution scans to delineate rebar, and a 750 MHz antenna pair for deep penetration. Nevertheless as a commercial product, the radar power output of the GPR Concrete Scanner is limited by the regulations of the Federal Communications Commission. For Army applications it is not necessary to adhere to these regulations, and increasing the power output will increase the penetration depth. Fortunately a rather simple circuit modification provides a power increase by a factor of 4-5 for the 750 MHz antennas. This modification could not be implemented for the 2 GHz antennas due to a component limitation in the commercial product design.

### Findings

After making the circuit modification, measurements indicate that the power output for the 750 MHz antennas was increased by a factor of 4.93. Since the amplitude of radar wave reflections attenuate as distance ( $r$ ) increases by the factor  $r^{-4}$ , the increased power increases the penetration depth by 49% for a lossless medium. The actual performance of the GPR on thick slabs is addressed in Section 2.5.

### 2.2 Microphone Array

An eight-channel microphone array was designed and installed on the bottom of the scanner (see Figure 6). The array is intended to support a variety of stress wave surveys including MASW, IE,

and tomographic surveys. A printed circuit board (PCB) was designed that contains the miniature microphones and their corresponding signal conditioning circuitry. The microphones are evenly distributed over a span of 17.5 cm, and a new bottom plate was created for the scanner with appropriately designed microphone apertures and a microphone PCB. The microphones respond to sound pressure levels in the range of 25 to 125 dB and have a frequency response of 20 Hz to 50 kHz. These ranges enable the array to be used with the wide variety of stress wave sources that are used in MASW, IE, and tomographic surveys. For the Phase I experiments, the conditioned microphone signals were connected to an external multi-channel audio recording system that recorded eight simultaneous 24-bit audio channels at 96,000 samples per second. The design and fabrication of an internal digitizer is planned for a future phase of this project.

## Findings

Rayleigh waves penetrate to depths of about a wavelength and have velocities ranging from 1200 to 2800 m/s in concrete, and therefore the selected 17.5 cm receiver span provides investigation to depths of 10 cm to more than a meter without spatial aliasing issues when using an appropriate source.

Laboratory tests were conducted to demonstrate that the microphone array has the ability to detect stress waves moving through the subsurface under the scanner. The scanner was placed on a concrete floor and the floor was struck with a hammer at a location five feet from the scanner. A large foam block was placed between the strike location and the scanner to absorb the direct air wave. The stress waves moving through the floor were clearly detected with different arrival times at each microphone.

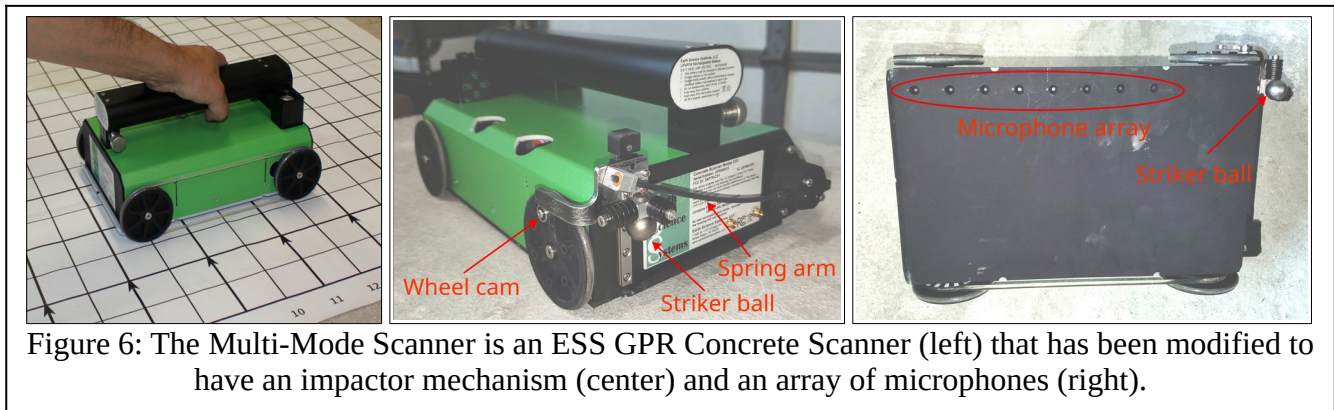


Figure 6: The Multi-Mode Scanner is an ESS GPR Concrete Scanner (left) that has been modified to have an impactor mechanism (center) and an array of microphones (right).

## 2.3 Stress Wave Excitation

Several methods for generating stress were investigated that are conducive to MASW and IE measurements. A mechanical impactor was added to the back of the unit and several iterations were built and tested until a solution was obtained that produced a sharp impact to the surface with minimal energy coupling to the microphone array through the sensor housing (see Figure 6). The impactor is a small steel ball on a flying carriage mechanism that can carry additional weights to enable changing the impact mass which changes the frequency content of the imparted stress waves. This spring loaded carriage mechanism is driven by a cam on the wheel of the scanner. Additionally, several different types of hand-held hammers were tested.

## Findings

For surface wave measurements, the source (impactor) should be far enough from the receivers such that they lie in the far-field region (more than a wavelength). In other words the distance between

the source and the scanner should be similar to the desired depth of investigation. For IE measurements, the source needs to produce energy at the ZGV-S1 resonant frequency. Using the Hertz elastic solution for the collision of two elastic objects (Sansalone and Carino, 1986), the half-sine impact period can be calculated for various hammers (see Table 2). For thick concrete structures (up to the project goal of 6 feet or 2 meters), this period should be about 500  $\mu$ s. Table 2 also contains estimated sound pressure levels at a microphone receiver array for various hammers based on computer simulations conducted by Zhu and Povovics (2008), and with typical ambient noise levels in urban areas of 60-70 dB the desired signal strength should be at least 75 dB.

One advantage to placing the impactor on the scanner is that continuous measurements can be made along a scan line. The disadvantages are that the scanner impactor is too close to the receiver array for deep surface wave surveys and it couples unwanted noise through the scanner housing. Also, the impact velocity of the scanner impactor is limited by the drive spring stiffness, which is in turn limited by the amount of resistance that can be driven by a wheel on the scanner. A separate hammer provides more flexibility in location, and different sized hammers can be easily selected as needed for IE surveys (see Figure 7 for example). A hand-held 2.5 lb (1.1 kg) hammer was used for large block MASW and IE experiments presented in Sections 2.6 and 2.8 below. Results from the scanner mounted impactor were inferior and often hard to interpret.

Table 2. Response of various hammers.

Hammer Type	Hammer Mass (kg)	Impact Velocity (m/s)	Impact Period ( $\mu$ s)	Impact Force (kN)	Sound Pressure (dB)
Ball impactor on scanner	0.062	2.38	254	0.582	77
2.5 lb hammer	1.14	10.0	503	22.6	120
5 lb sledge	2.27	10.0	633	35.9	131
Rubber mallet	0.45	10.0	8,687	0.523	75

## 2.4 Construct Large Concrete Structures

Two sets of large concrete blocks were built to evaluate the Multi-Scanner (see Figures 7 and 8). The first set was poured using three 8 x 8 x 5 foot forms (2.44 x 2.44 x 1.52 meters) each with different mixes to achieve different concrete strengths (although one of the forms collapsed during pouring). Several steel rebar targets were anchored in the forms before pouring. These blocks have been used for MASW and IE tests, and will be used for GPR testing after they have fully cured. The second set of large blocks was built using small heavy-weight solid-concrete blocks constructed according to ASTM C90 that measure 4 x 8 x 16 inches (10 x 20 x 40 cm), which were stacked into large blocks with nominal sizes of 5.3 x 2 x 3.3 feet (1.6 x 0.6 x 1.0 meters) and 4.5 x 2 x 6.6 feet (1.4 x 0.6 x 2.0 meters). A one-inch wide (2.5 cm) strip of copper tape was placed between blocks at various depths to provide a radar wave reflector that is very similar to actual steel rebar. This second set of stacked blocks is used for GPR testing but is not suitable for elastic wave tests due to the stress-strain discontinuities between the small blocks. A small block with metallic fibers was also fabricated.

## Findings

The large concrete blocks were poured on October 13, 2022 using cement type I/II (no slag), fly ash class C, and other parameters as listed in Table 3. A small test cylinder was prepared using the mix used for each of the large blocks, and after curing for 28 days compression tests were made on sample

to determine the strength of each concrete mixture (see Table 3). The form for block P2 collapsed while being poured because the pour was too fast and block was lost.

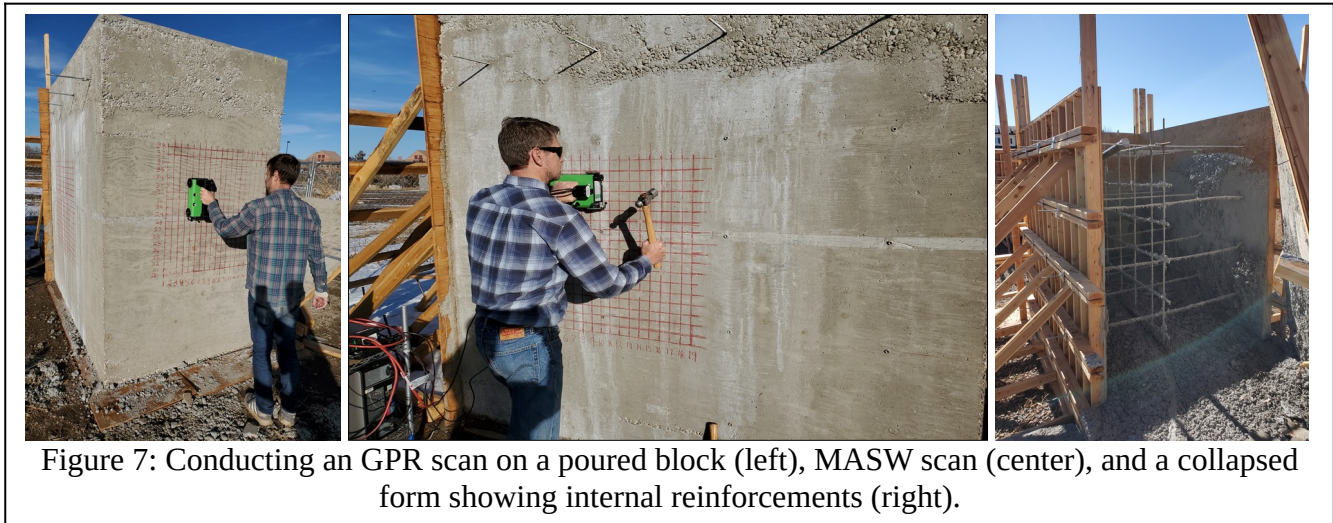


Figure 7: Conducting an GPR scan on a poured block (left), MASW scan (center), and a collapsed form showing internal reinforcements (right).

Table 3. Parameters of poured concrete blocks.

Block Number	Fiber content	Target Strength	Water / Concrete Ratio	28 Day Strength Test
P1	None	2500 psi (17 MPa)	0.73	3603 psi (24.8 MPa)
P2 (collapsed)	High	5000 psi (34 MPa)	?	N/A
P3	Low	3500 psi (24 MPa)	0.62	4757 psi (32.8 Mpa)

There was an administrative delay that needed to be rectified before the large blocks were constructed, which left a small window for conducting the surveys. Both stress wave and GPR surveys were conducted 28 days after pouring, but the GPR penetration into the poured concrete blocks was very low because the concrete had not yet cured sufficiently to be transparent to radar waves. This necessitated construction of the stacked blocks for evaluating the GPR performance. To test the penetration depth of the GPR on well-cured concrete, stack block structures were constructed from smaller blocks with dimensions listed in Table 4. To simulate linear metallic objects such as rebar, a 1" wide copper tape was placed vertically in the block (see Figure 8).

Table 4. Dimensions of composite block structures used to test GPR penetration depth.

Block Number	Nominal Block Dimensions (W x H x D)	Individual Block Thickness	Measured Depth to Vertical Tape Reflector	Measured Thickness
S1	64" x 24" x 40" (160 x 60 x 100 cm)	8" (20 cm)	15.5" (39.4 cm)	38.5" (97.8 cm)
S2	64" x 24" x 40" (160 x 60 x 100 cm)	8" (20 cm)	23" (58.4 cm)	38.5" (97.8 cm)
S3	54" x 24" x 80" (140 x 60 x 200 cm)	16" (40 cm)	32" (81.3 cm)	78" (198.1 cm)
S4	54" x 24" x 80" (140 x 60 x 200 cm)	16" (40 cm)	46" (116.8 cm)	78" (198.1 cm)

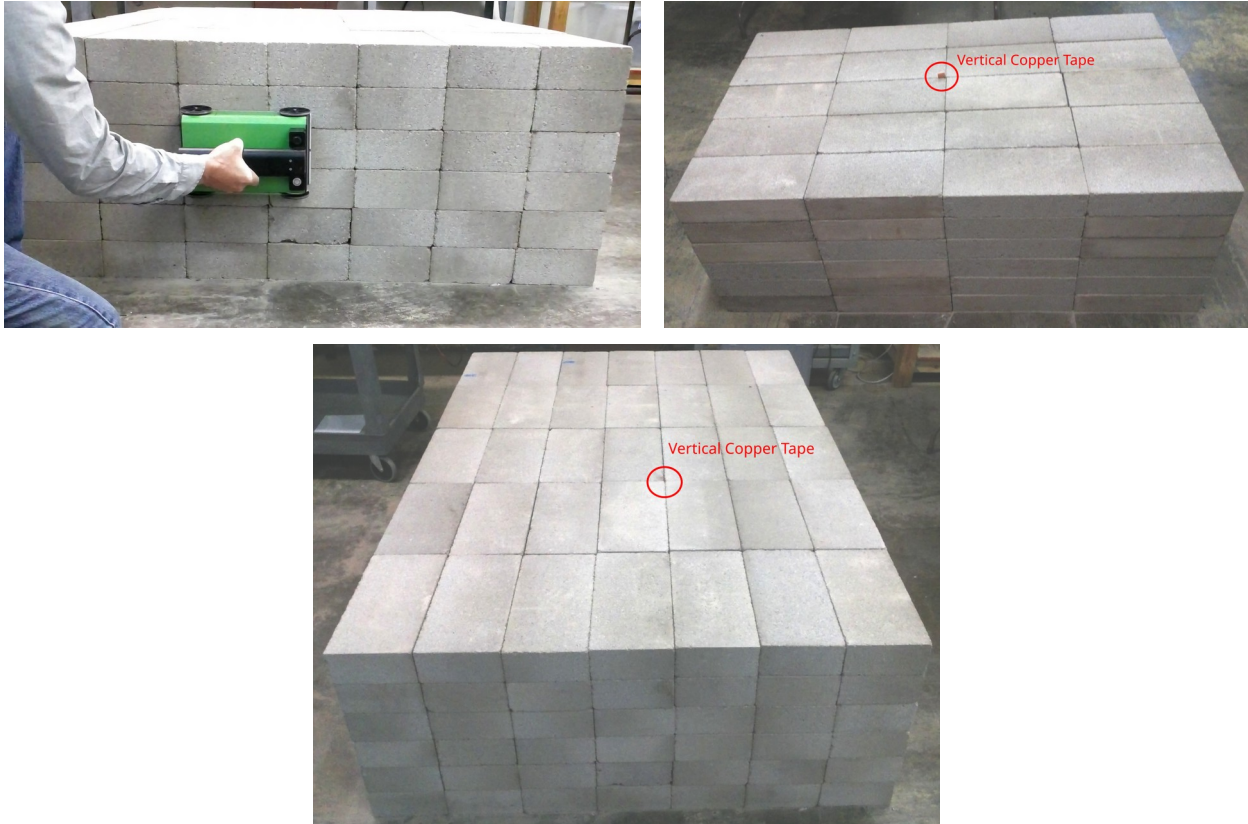


Figure 8: Conducting a GPR scan on the composite block (top left), composite block S2 with vertical copper strip (top right), and composite block S3 with vertical copper strip (bottom).

A small 24 x 12 x 6 inch (61 x 30 x 15 cm) concrete block was cast to test the GPR response to metal fibers (see Figure 9). A small rebar grid was placed at the bottom of the block, and the mix was Quikrete high strength concrete with 25 lbs/yard<sup>3</sup> (15 kg/m<sup>3</sup>) of steel fibers.



Figure 9: Form for a small concrete block with a rebar grid (left), and completed block that was cast using a mix containing metallic fibers (right).

## 2.5 Demonstrate GPR Performance

The Multi-Mode Scanner's GPR system was tested to verify that it can detect the back of a six foot thick slab and detect rebar to depths of at least three feet. Tests were made using the large stacked block structures, on a pre-existing two foot (60 cm) thick reinforced floor designed to support heavy loads, and on a large poured concrete block.

### Findings

Results from GPR tests conducted using the stacked blocks S1 and S2 are shown in Figure 10 where the scan results from a 38.5 inch (98 cm) thick blocks with linear metallic reflectors at 15.5" (39.4 cm) and 23" (58.4 cm) deep. Figure 11 shows results from 78 inch (198 cm) thick blocks with linear metallic reflectors at 32" (81.3 cm) and 46" (116.8 cm) deep. These cross-section images were obtained using the 2 GHz GPR antennas with the standard commercial radar power output. The travel-time to depth conversion was made by fitting a hyperbola to the linear metallic reflector to determine the dielectric constant ( $\epsilon_r = 4.8$ ) and the corresponding radar wave velocity. The reflection from the back of the blocks is evident along with multiple reflections from the back and sides of the block. These multiple reflections have traveled further than the reflection off the back surface indicating that the waves can penetrate farther than the block thickness. The proxy rebar reflector is quite bright even at 46" (116.8 cm) depth, however the tails of the hyperbolic reflection have less slope for deeper reflectors which makes it slightly more difficult to precisely locate the apex or lateral location of the reflector, and the reflections from deep closely spaced objects may interfere. The reflector depths indicated on these cross sections are within 7% of the actual values and are well within the stated goal of one foot, and the goal to penetrate to a depth of 6 feet (1.83 m) is clearly met. This penetration depth may not be possible in all concrete materials, and cross-sections from surveys on concrete bodies with coarse aggregate or dense rebar may have shallow reflections that obscure deeper reflections. The faint reflections from the cracks between the smaller blocks illustrates GPR's ability to locate voids, but in general small cracks and voids will often escape detection with GPR.

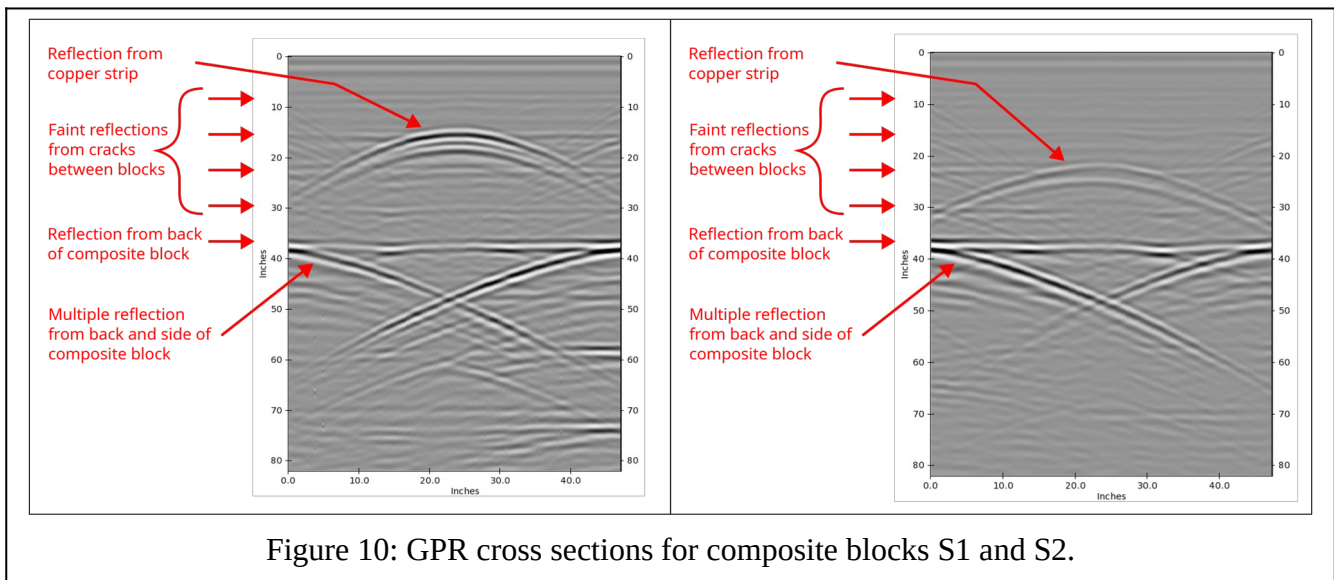


Figure 10: GPR cross sections for composite blocks S1 and S2.

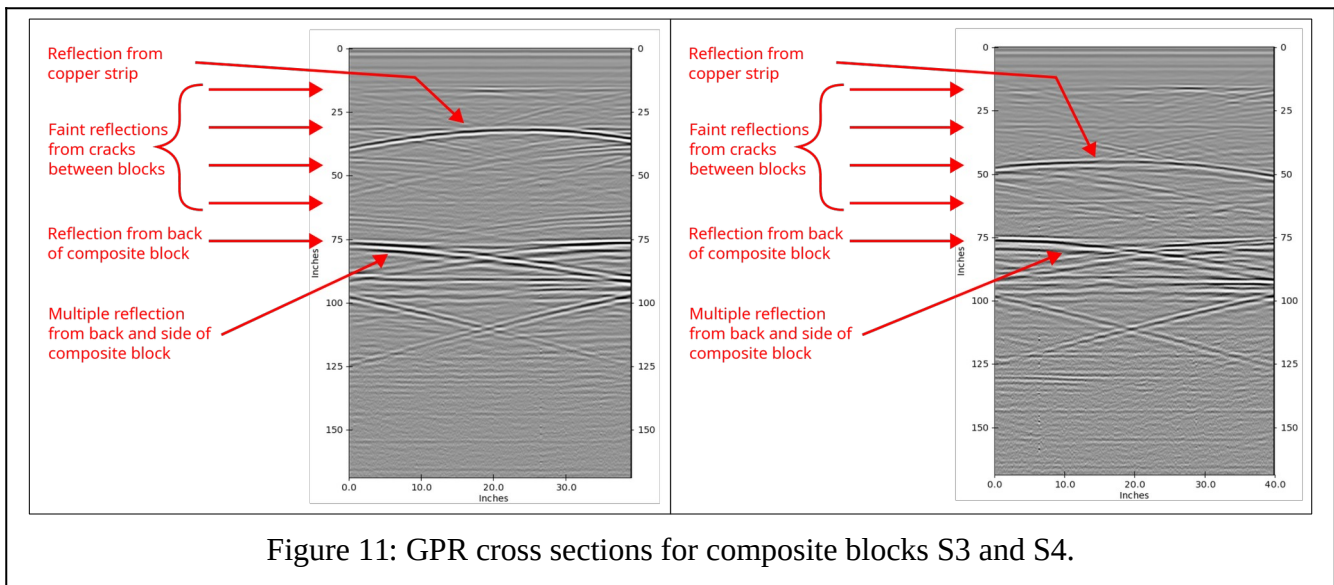


Figure 11: GPR cross sections for composite blocks S3 and S4.

Figure 1 shows the 2 GHz GPR results from a two foot thick reinforced floor. The travel-time to depth conversion was made by fitting a hyperbola to a rebar reflection to determine the dielectric constant ( $\epsilon_r = 5.5$ ) and radar wave velocity. By observing reflection locations on cross-section images, the rebar diameter of 0.86 inches (2.2 cm) was determined by subtracting the depth between crossing bars, the spacing between bars was 12" (30 cm), and the thickness of the slab was 2.1 feet (61 cm). The exact values of these parameters are unknown, but the measured values are consistent with scaled drawings for the building.

The GPR surveys conducted on the poured blocks suffered from the large attenuation of incompletely cured concrete. The surface-coupled GPR antennas in the Multi-Mode Scanner were designed to couple to surfaces with dielectric values in the range of 3 to 7, and higher dielectric values cause an impedance mismatch which results in ringy waveforms. Figure 12 shows the 750 MHz GPR cross sections from block P3, where the ringing in the waveforms are evident on the left section. In the right section the ringing was removed by calculating the average waveform for the cross-section and subtracting it from all traces in the section (this is a standard GPR processing step). No hyperbolic reflections were available for measuring the dielectric constant, so a value ( $\epsilon_r = 12$ ) was selected to place the reflection at a nominal depth of 5 feet (1.52 m). This large dielectric value is indicative of saturated and incompletely cured concrete. The reflectors at about 2.1 feet (67 cm) are from rebar that was placed inside the forms (see Figure 7). These rebar reflections do not present the typical hyperbolic shapes because 1) many of the bars are oriented parallel to the section rather than transverse, 2) there are multiple bars in close proximity, and 3) the poor resolving capability of the relatively low frequency 750 MHz radar. The 2 GHz radar was not able to detect the rebar or the back surface, but can provide more resolution when the concrete has fully cured. The ability to detect the back wall reflection through 5 feet (1.52 m) of partially cured concrete is notable. The thickness indicated by the cross-section changes by about 6% along the scan line due to changing moisture content or state of curing in the concrete along the scan line, which changes the velocity of the wave.

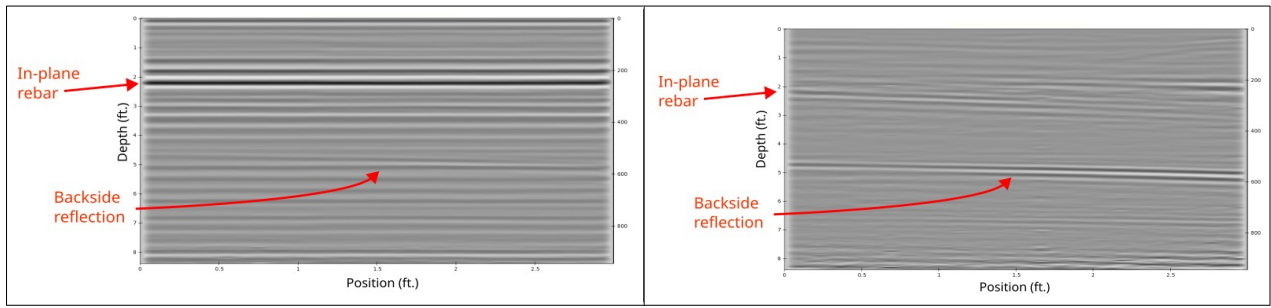


Figure 12: GPR cross-sections from 750 MHz antennas for poured block P3, with the depth corrected section on the left, and the same section with background correction on the right.

## 2.6 Surface Wave Performance

MASW surveys were conducted on the large poured blocks using the external audio recording system. Two surveys were made on each block (P1 and P3), one with the microphone array oriented vertically and another with the array oriented horizontally. In each case a hand-held 2.5 pound (1.1 kg) steel hammer was used with an impact point one foot (30 cm) from the scanner. A data parsing routine was created to extract short snippets from the recorded microphone traces corresponding to the hammer blows. Thresholds for detecting the hammer blows were determined experimentally, and the extracted data had to be manually inspected. This step will be completely automated in a future phase by adding a hardware strike detector to the hammer.

Using the extracted microphone signals, surface wave velocities were determined by generating a coherence image and dispersion curve as described in Section 1.2. To obtain a single representative value for Rayleigh velocity, the median value of the dispersion curve was calculated using frequencies above 4.6 kHz. Because plate modes A0 and S0 (i.e., Lamb waves) converge to within 1% of Rayleigh velocity at frequency-thickness products above 7000, a slab thickness of 5 feet (1.5 m) corresponds to minimum valid frequency of 4.6 kHz.

### Findings

The repeated experiments produced representative Rayleigh velocities with a mean difference of 2.2%, indicating that the measurement is repeatable and reliable. Although these results were obtained from a small number of tests, the Multi-Mode Scanner and software benefit significantly from MASW instrumentation and software technology previously developed by ESS. The representative Rayleigh velocity is used as a basis for calculating elastic properties of the concrete.

## 2.7 Estimating Elastic Properties

Using the Rayleigh wave velocities determined from scans on the large poured blocks, the compressional wave velocity, modulus of elasticity, and concrete strength were estimated using the methods discussed in Section 1.3.

### Findings

Table 5 lists the measured Rayleigh velocity, calculated shear velocity, calculated compressional velocity, calculated Young's modulus, calculated concrete strength, and the 28 day strength test results. The strength tests were made by casting cylinders of the concrete mix material

used to pour the large blocks, which were then destructively tested to determine compressive strength after they had cured for 28 days. The largest difference between calculated and measured strength was 636 psi (4.4 MPa) and the mean difference is 302 psi (2.1 MPa), which is well within the stated goal of +/- 3,000 psi (21 MPa). Unfortunately the planned tests using the large poured block with high fiber content were not possible because the form collapsed while it was being poured.

Table 5. Measured Rayleigh velocity, calculated concrete strength, and 28 day strength test results.

Block Number	Scanner Alignment	Measured Rayleigh Velocity	Calculated Shear Velocity	Calculated Compress. Velocity	Calculated Young's Modulus	Calculated Concrete Strength	28 Day Strength Test
P1	Vertical	6752 ft/s 2058 m/s	7563 ft/s 2305 m/s	11345 ft/s 3458 m/s	3486 ksi 24.0 GPa	3676 psi 25.4 MPa	3603 psi 24.8 MPa
P1	Horizontal	6877 ft/s 2096 m/s	7703 ft/s 2348 m/s	11554 ft/s 3522 m/s	3622 ksi 25.0 GPa	3967 psi 27.4 MPa	3603 psi 24.8 MPa
P3	Vertical	6939 ft/s 2115 m/s	7773 ft/s 2369 m/s	11659 ft/s 3554 m/s	3691 ksi 25.5 GPa	4121 psi 28.4 MPa	4757 psi 32.8 MPa
P3	Horizontal	7126 ft/s 2172 m/s	7982 ft/s 2433 m/s	11973 ft/s 3650 m/s	3908 ksi 26.9 GPa	4619 psi 31.8 MPa	4757 psi 32.8 MPa

## 2.8 Impact Echo Performance

Using the recorded microphone data from the large poured concrete slabs, the thickness was calculated using the method described in Section 1.4. Tests were also conducted on a structurally strong floor of an existing building.

### Findings

Table 6 lists the thickness measured using the IE method. The measured thicknesses are within the stated goal of +/- one foot. For the case of the largest error (0.49 ft, 0.15 m), the spectral density curve has a second peak very near the highest peak whose frequency value would result in a smaller error. All of the calculated thicknesses are greater than the actual thicknesses, which may be due to an error in calculating the compressional velocity or measuring the Rayleigh velocity. The maximum error was 18.5 % and the mean error was 8.6 %. The actual thickness of the strong floor was not measured, but is inferred from building plans. In the tests to date, the thicknesses determined from GPR data are more accurate than those determined using the IE method.

Table 6. Measured slab thickness using the IE method.

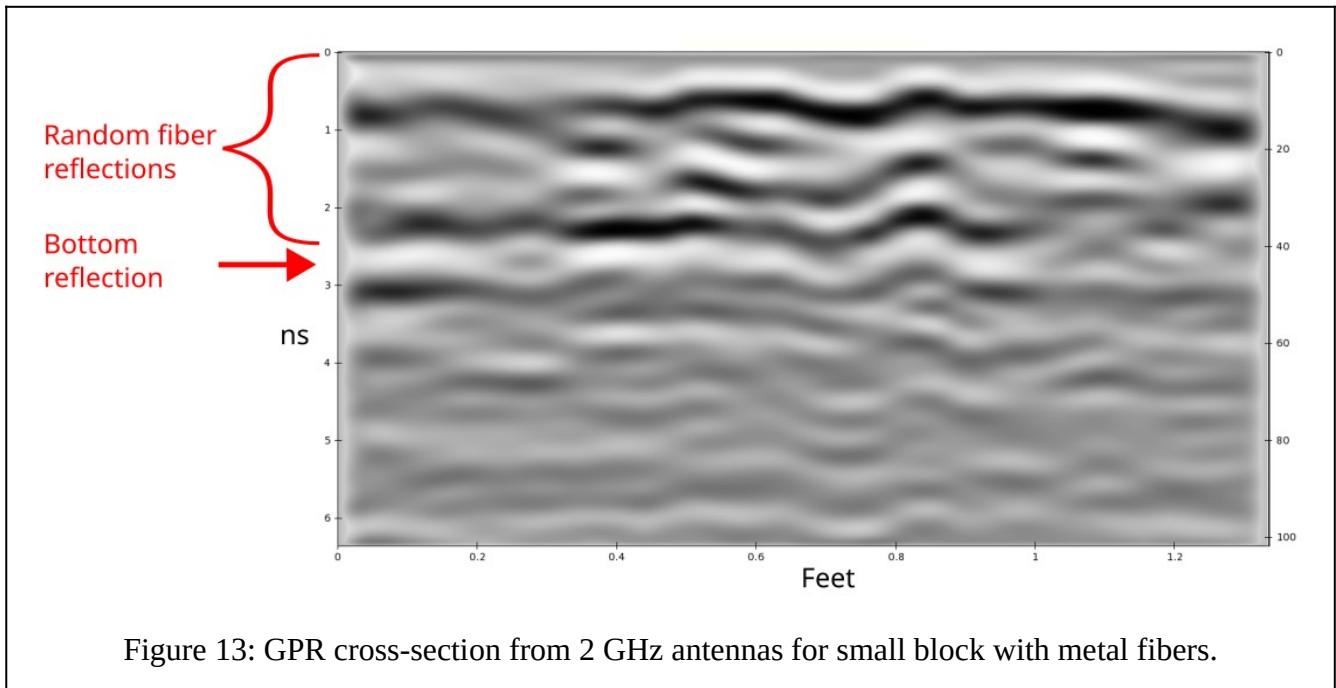
Block Number	Scanner Alignment	Measured Thickness	Actual thickness
P1	Vertical	5.08 ft, 1.55 m	5 feet, 1.52 m
P2	Horizontal	5.49 ft, 1.67 m	5 feet, 1.52 m
P3	Vertical	5.13 ft, 1.56 m	5 feet, 1.52 m
P3	Horizontal	5.27 ft, 1.61 m	5 feet, 1.52 m
Strong floor	Vertical	2.28 (0.69 m)	2 feet (0.61 m), inferred
Strong floor	Horizontal	2.37 (0.72 m)	2 feet (0.61 m), inferred

## 2.9 Detecting the Presence of Metal Fibers

The addition of fiber reinforcement into concrete mixes can greatly increase their strength. Strength values for plain concrete without reinforcement is less than 5000 psi (34 MPa), and greater values imply the presence of reinforcement. If metal fibers are used for reinforcement, they cause a characteristic signature in GPR scans that can be readily identified. If non-metallic fibers are used, their presence can be inferred from strength estimates derived from surface wave surveys when the value is larger than 5000 psi (34 MPa).

### Findings

A small 24 x 12 x 6 inch (61 x 30 x 15 cm) concrete block was fabricated with a mix containing metallic fibers as described in Section 2.4 and shown in Figure 9. The cross-section from the GPR scan using the 2 GHz antennas is shown in Figure 13, where the random arrangement of fibers causes reduced penetration depth and severe distortion reflections from rebar and bottom of slab. There are random bright reflectors from the metallic fibers that do not have the characteristic hyperbolic pattern of rebar, nor the linear patterns of the back side reflection. The presence of shallow random bright reflectors can be used to indicate the presence of metallic fibers.



## 2.10 Expediency of Scan

The MASW and IE echo scans to measure Rayleigh wave velocity and slab thickness can be done in about 10 seconds. A single GPR scan line that produces a 2D cross-section can also be made in about 10 seconds. However, a high resolution 3D GPR scan requires about five minutes after a scan grid has been setup. The scan grid provides a guide for users to run the scanner on regularly spaced scan lines in a crosshatch pattern. A 3D scan is needed to find and map all of the rebar under a scan area, and since it is not practical to conduct a high resolution 3D scan over the entire area, the scan is limited to a smaller representative area.

## Findings

Figure 14 below shows a 3 x 3 foot (91 x 91 cm) printed scan mat that can be quickly and easily placed on horizontal surfaces. It is often difficult to affix the mat to vertical concrete surfaces unless the surface is very clean. Users can use wax or paint markers to draw a scan grid, but this is a time consuming process that may require 15 minutes or more. The advantage of drawn grids is that they can be made at any shape (aspect ratio) and line spacing, whereas scan mats have a fixed pattern.

A number of commercially available quick set adhesives were tested to determine suitability for affixing a scan mat to a vertical concrete surface. Dirty and dusty concrete surfaces are common, and none of the tested adhesives worked well on uncleaned surfaces. Better results were obtained after cleaning the concrete in areas at the corners of the mat with isopropyl alcohol before applying the adhesive. The process of cleaning and applying adhesive to affix a scan mat requires at least five minutes and necessitates adding depletable cleaning supplies to the survey kit.

To facilitate conducting a 3D scan expeditiously, a method is needed for quickly deploying a scan grid with any shape (aspect ratio) on any surface – regardless of its orientation. For this reason, future work will investigate using camera based methods for providing scan grid guidance.

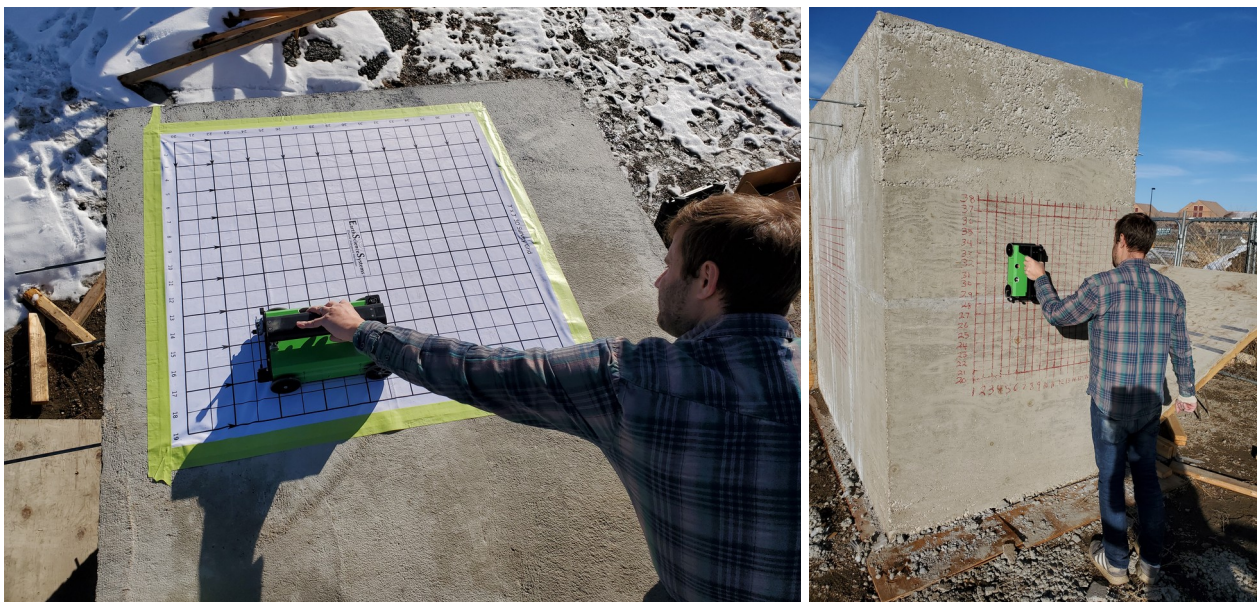


Figure 14: GPR scanning with scan grid on printed mat (left) and drawn scan grid (right).

## 3 Conclusions

A prototype Multi-Mode Scanner has been built and successively tested. Various concrete structures were built for testing and evaluating the new scanner. In preliminary testing, all of the Army's stated goals have been met, and a summary of the target metrics is presented in Table 7. Both the GPR and IE methods were able to reach the thicknesses indicated without reaching the limit of the measurement range. Strength estimates are well within the stated goals, but further tests are needed on very high strength structures. The ability to detect rebar to depth of four feet was successfully demonstrated, and deeper detection is possible however it may be difficult to resolve individual bars. The system is lightweight, portable, and produces results quickly. Placing a scan grid pattern on a

horizontal surface can require additional setup time, and a new method to address this issue is planned for future work.

Table 7. Target performance metrics and actual results.

Metric	Goal	Test Results	Comments
GPR investigation depth	6 ft	Success at 6.6 ft.	Tests did not reach limit
IE investigation depth	6 ft	Success at 5 ft	Tests did not reach limit
Strength	3 to 30 +/- 3 ksi	636 psi max error 302 psi mean error	Only tested 3606 and 4757 psi materials
GPR Thickness	Up to 6 +/- 1 feet	Accuracy 7%	Based on velocity from hyperbola
IE Thickness	Up to 6 +/- 1 feet	0.49 ft. max error 0.25 ft. mean error	Sloped walls nominally 5 ft. thick
Map rebar position and depth	Estimate density of steel reinforcement	Depth accuracy 7% Position accuracy 5%	Adversely affected by rough surface, decreasing accuracy with depth
Detect (steel) fibers	Estimate density of fiber reinforcement	Steel fiber detected by GPR image texture	Non-metallic fiber inferred from high strength estimate
Size	Hand held	12 x 8.9 x 8.5 inches (30.5 x 35.6 x 21.6 cm)	
Weight	Light weight	5 lbs. (2.3 kg)	
Survey time	Rapid non-destructive assessment	5 minutes	Does not include time to place scan mat

Future work will focus on developing a production ready system that is very easy to use. Further development of the tablet PC software will make the system more capable and easier to use, and will report all the structural parameters presented in Table 7. A significant effort will focus in field testing, demonstration, and training. Finally, the new product will be commercialized and added to the existing ESS product line.

## 4 References

- American Concrete Institute, 2017, 318-05: Building Code Requirements for Structural Concrete and Commentary, ISBN 9780870311796, 430 pp.
- Gibson, A., and Popovics, J., 2005, Lamb Wave Basis for Impact-Echo Method Analysis, *Journal of Engineering Mechanics*, 131:4 (438).
- Groschup, R., and Grosse, C., 2015, Enhancing Air-Coupled Impact-Echo with Microphone Arrays, *International Symposium on Non-Destructive Testing in Civil Engineering (NDT-CE)*, September 15 - 17, Berlin, Germany.
- He, H., and Senetakis, K., 2016, A Study of Wave Velocities and Poisson Ratio of Recycled Concrete Aggregate, *Soils and Foundations*, v. 56, n. 4, p. 593-607.
- Lee, B. J., Kee, S. H., Oh, T., and Kim, Y. Y., 2017, Evaluating the Dynamic Elastic Modulus of Concrete Using Shear-Wave Velocity Measurements, *Advances in Materials Science and Engineering*, v. 2017, Article ID 1651753, 13 pp.
- Park, J.Y., Yoon, Y.G., and Oh, T.K., 2019, Prediction of Concrete Strength with P-, S-, R-Wave Velocities by Support Vector Machine (SVM) and Artificial Neural Network (ANN), *Applied Sciences*, v. 9, n. 19: 4053, <https://doi.org/10.3390/app9194053>.
- Sabbag, N. and Uyanik, O., 2017, Prediction of Reinforced Concrete Strength by Ultrasonic Velocities, *J. Applied Geophysics*, v. 141, p. 13-23.
- Sansalone, M., and Carino, N., 1986, *Impact-Echo: A Method for Flaw Detection in Concrete Using Transient Stress Waves*, NBSIR 86-3452, National Bureau of Standards, Washington, D.C.
- Trtnika, G., Kavčič, F., and Turk, G., 2009, Prediction of Concrete Strength using Ultrasonic Pulse Velocity and Artificial Neural Networks, *Ultrasonics*, v. 49, n. 1, p. 53-60.
- Vu, C., Weiss, J., Plé, O., and Amitrano, D., 2021, *The Potential Impact of Size Effects on Compressive Strength for the Estimation of the Young's Modulus of Concrete*, Materials and Structures, Springer Verlag, fhal-03378082f.
- Zhu, J., and Popovics, J., 2006, Non-contact NDT of Concrete Structures Using Air Coupled Sensors, Newmark Structural Engineering Laboratory Report Series 010, ISSN 1940-9826, <http://hdl.handle.net/2142/5320>.

## 5 Abbreviations and Acronyms

2D	Two-dimensional
3D	Three-dimensional
A0	First Antisymmetric Mode
cm	Centimeter
CU	University of Colorado
dB	Decibel
ESS	Earth Science Systems, LLC
ft	feet
GHz	Giga Hertz
GPa	Giga Pascal
GPR	Ground Penetrating Radar
IE	Impact Echo
kg	Kilogram
kHz	Kilo Hertz
lb, lbs	Pounds
m	Meter
MASW	Multi-channel Analysis of Surface Waves
MHz	Mega Hertz
MPa	Mega Pascal
ns	Nanoseconds
PCB	Printed Circuit Board
psi	Pounds per Square Inch
s	Seconds
S0	First Symmetric Mode
ZGV-S1	Zero-Group-Velocity first-Symmetrical-mode (Lamb wave)